Properties of the quarter-wave Bragg reflection waveguide: theory

Brian R. West and Amr S. Helmy

Edward S. Rogers Sr. Department of Electrical and Computer Engineering, University of Toronto, 10 King's College Road, Toronto, Ontario, Canada M5S 3G4

Received October 13, 2005; revised December 13, 2005; accepted December 19, 2005; posted January 10, 2006 (Doc. ID 65329)

The Bragg reflection waveguide (BRW), or one-dimensional photonic crystal waveguide, has recently been proposed for a wide spectrum of applications ranging from particle acceleration to nonlinear frequency conversion. Here, we conduct a thorough analytical investigation of the quarter-wave BRW, in which the layers of the resonant cladding have a thickness corresponding to one quarter of the transverse wavelength of a desired guided mode. An analytical solution to the mode dispersion equation is derived, and it is shown that the quarter-wave BRW is polarization degenerate, although the TE and TM mode profiles differ significantly as the external Brewster's angle condition in the cladding is approached. Analytical expressions for waveguide properties such as the modal normalization constants, propagation loss, and overlap factors between the mode and each waveguide layer are derived, as are dispersion and tuning curves.

OCIS codes: 130.3120, 230.7370, 230.1480.

1. INTRODUCTION

Increased device functionality is a prerequisite for the next generation of optical networks, as well as the emerging fields of biophotonics, optical networks, optical sensing and signal processing, and microwave photonics. To achieve certain propagation properties while accommodating the dispersive properties of optical materials, it has become necessary to move away from the common total internal reflection (TIR) waveguide and instead investigate the use of resonant-cladding waveguides. There has been much promise in the properties afforded by photonic bandgap waveguides; however, implementations have been disappointing owing to practical issues such as lithographic accuracy and scattering losses. Also as important is the fact that the waveguiding properties have been engineered, to date, chiefly through two-dimensional planar photonic bandgap structures. Although these provide some control over the propagation properties, some of these characteristics are still determined by the lateral TIR structures. Therefore, the need still exists for versatile, low-loss waveguides that provide control over guiding properties such as mode size, group-velocity dispersion, and effective index tunability and maintain single-mode operation while controlling mode shapes, etc. The Bragg reflection waveguide (BRW) has recently emerged as a strong contender for these applications. However, a thorough analytical investigation has not been available to date, to the best of our knowledge.

The BRW was first analyzed in detail by Yeh and coworkers.[1,2] In this structure, transverse waveguiding is achieved not by TIR but by distributed reflection within a periodic cladding. As such, the guided modes can have effective indices lower than all material indices—and even less than unity—provided that the transverse propagation vector lies within the Bragg stop band of the cladding. This phenomenon has provided increased functionality of photonic devices, for instance, in electron accelerators,[3,4] and phase matching for nonlinear frequency conversion.[5] In addition, BRWs have been proposed for applications such as mechanically tunable air-core filters,[6] polarization splitters,[7] and soliton propagation.[8]

The quarter-wave BRW (QtW-BRW) is a special case in which the cladding layers have an optical thickness equal to one quarter of the wavelength with respect to the transverse propagation vector of the guided mode. This constraint serves to place the guided mode in the center of the stop band, maximizing the confinement in the core. Yeh derived basic properties of the quarter-wave stack for normal incidence and in the case of a mode confined near the interface between two periodic claddings (with no core).[9] However, to the best of our knowledge, no previous work has been carried out on systematic determination of analytical expressions for the properties of the QtW-BRW. Such expressions are of great benefit to the design community in that they reduce reliance on complex and expensive numerical modeling tools. As will be demonstrated in this work as well, a careful investigation of waveguiding for TM polarization, which has not been previously analyzed, leads to the identification of two regimes of operation for the TM mode, depending on the relative magnitudes of the ray angle and exterior Brewster's angle in the cladding. This has tremendous promise in the design of highly polarization-selective devices. This analysis also shows that the QtW-BRW is polarization degenerate, a property that can be exploited in quantum optical applications, such as the efficient generation of polarization-entangled photon pairs.[10]

In this work, we derive analytical formulas for several important properties of the one-dimensional (slab) QtW-BRW. In Section 2, we follow the formalism of Yeh to derive the mode dispersion equation for the general (non-QtW) BRW but extend the derivation to include both TE and TM modes. The mode dispersion equation is then

subjected to the quarter-wave constraint in Subsection 2.C, with subsequent solution of the normalized guided modes. In Section 3, we derive analytical expressions for several properties of the waveguide—modal overlap factors with each region of the waveguide, propagation loss in a cladding of finite thickness, and first-order chromatic dispersion of the mode. Section 4 will introduce an analytical approximation to the tuning curves of the effective index through a perturbation of the core index. Calculation of tuning and dispersion is facilitated through the development of a generalized first-order perturbation theory in Appendix A. Finally, in Section 5, we will extend the analysis to the practical case of two-dimensional channel waveguides, in which transverse confinement is provided by TIR.

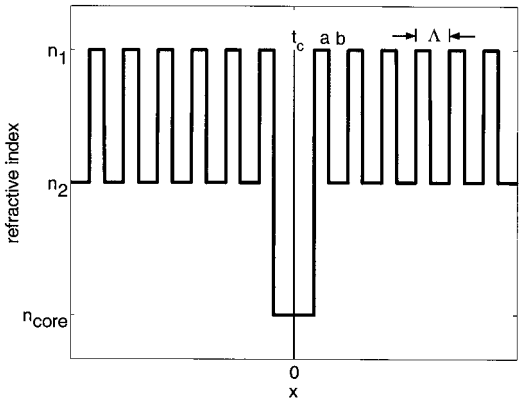

Fig. 1. Index profile of a one-dimensional BRW.

2. MODE DISPERSION EQUATION OF THE QUARTER-WAVE BRAGG REFLECTION WAVEGUIDE

The one-dimensional general BRW is shown in Fig. 1. By convention, the cladding consists of slabs of index n_1 (thickness a) and n_2 (thickness b), with $n_1 > n_2$, and n_1 is closest to the core. The core has thickness t_c and index n_c. For most applications, n_c is less than n_2, although this is not strictly necessary for Bragg waveguiding, as will be shown below. The cladding is assumed to contain an infinite number of periods; the effect of a large but finite number of periods will be discussed as a special case. Guided-mode propagation is along z, and we assume that $\partial/\partial y = 0$. The electric field can thus be written as[1]

$$E(x,y,z,t) = E(x)\exp[i(\omega t - \beta z)], \tag{1}$$

where $\beta = 2\pi n_{\text{eff}}/\lambda = k_0 n_{\text{eff}}$ is the propagation constant, n_{eff} is the modal effective index, and $E(x)$ is the transverse field envelope, which satisfies the equation

$$\frac{\partial^2 E(x)}{\partial x^2} + k^2(x)E(x) = 0. \tag{2}$$

The term $k(x)$ is the transverse propagation vector, which takes on discrete values in each slab,

$$k_i = k_0\sqrt{n_i^2 - n_{\text{eff}}^2}. \tag{3}$$

We shall concentrate on symmetric waveguides, for which $n(-x) = n(x)$. In this case, the guided modes possess either even or odd symmetry. Although the BRW may support several modes, only one will be at the quarter-wave condition, and it is unlikely that other modes will fall within the cladding stop band.[2] Thus, we concentrate on only the lowest-order mode for each polarization and note that the derivation of higher-order modes proceeds in a similar fashion.

A. Transverse-Electric Polarization

For a slab waveguide in which the x direction is normal to the substrate and propagation is defined to be along the z axis, the TE mode has field components E_y, H_x, and H_z, with all other components equal to zero. Only one component is independent, with the others determined by Maxwell's curl equations. We will thus concern ourselves only with E_y. For the lowest-order mode, we can assume a field envelope of the form[9]

$$E_y(x) = \begin{cases} C_1^{\text{TE}}\cos(k_c x), & |x| \le \dfrac{t_c}{2} \text{ (core)} \\ C_2^{\text{TE}} E_{K,\text{TE}}\left(|x| - \dfrac{t_c}{2}\right)\exp\left[iK_{\text{TE}}\left(|x| - \dfrac{t_c}{2}\right)\right] & |x| > \dfrac{t_c}{2} \text{ (cladding)} \end{cases}, \tag{4}$$

where C_i are polarization-dependent constants to be determined, k_c is the transverse wave vector in the core layer, and K_{TE} is the Bloch wave vector, defined below. The assumption of an infinite cladding implies that β is real (absorption in the waveguide is presumed negligible here). For ease of notation, we will consider only the region $x \ge 0$ and note that $E(-x) = E(x)$ by symmetry. According to the Floquet theorem, $E_{K,\text{TE}}(x)$ is periodic with period $\Lambda = a + b$, which can be denoted

$$E_{K,\text{TE}}(x + \Lambda) = E_{K,\text{TE}}(x). \tag{5}$$

The properties of the field in the cladding have been examined extensively by Yeh[9] and are reproduced here using the coordinate system of Fig. 1. For an infinite periodic stack, the electric field in the nth unit cell (n $= 0, 1, 2\ldots$, where the zeroth unit cell is adjacent to the waveguide core) can be written as the sum of incoming and outgoing waves,

$$E_{\mathrm{clad}}(x)=\begin{cases} a_{\mathrm{n,TE}}\exp\left[ik_1\left(x-\frac{t_c}{2}-\mathrm{n}\Lambda\right)\right]+b_{\mathrm{n,TE}}\exp\left[-ik_1\left(x-\frac{t_c}{2}-\mathrm{n}\Lambda\right)\right], & \mathrm{n}\Lambda\leqslant\left(x-\frac{t_c}{2}\right)\leqslant\mathrm{n}\Lambda+a \\ c_{\mathrm{n,TE}}\exp\left[ik_2\left(x-\frac{t_c}{2}-\mathrm{n}\Lambda-a\right)\right]+d_{\mathrm{n,TE}}\exp\left[-ik_2\left(x-\frac{t_c}{2}-\mathrm{n}\Lambda-a\right)\right], & \mathrm{n}\Lambda+a\leqslant\left(x-\frac{t_c}{2}\right)\leqslant(\mathrm{n}+1)\Lambda \end{cases}, \quad (6)$$

where the amplitudes a_n, b_n, c_n, and d_n are to be determined. In the cladding regions of index n_1, these are related between adjacent unit cells by a unimodular field-transfer matrix,

$$\begin{pmatrix} a_{n-1} \\ b_{n-1} \end{pmatrix}_{\mathrm{TE}}=\begin{bmatrix} A & B \\ C & D \end{bmatrix}_{\mathrm{TE}}\begin{pmatrix} a_n \\ b_n \end{pmatrix}_{\mathrm{TE}}. \quad (7)$$

The matrix elements for TE polarization are

$$A_{\mathrm{TE}}=\exp(ik_1a)\left[\cos k_2b+\frac{i}{2}\left(\frac{k_2}{k_1}+\frac{k_1}{k_2}\right)\sin k_2b\right],$$

$$B_{\mathrm{TE}}=\exp(-ik_1a)\left[\frac{i}{2}\left(\frac{k_2}{k_1}-\frac{k_1}{k_2}\right)\sin k_2b\right],$$

$$C_{\mathrm{TE}}=B_{\mathrm{TE}}^{*},\quad D_{\mathrm{TE}}=A_{\mathrm{TE}}^{*}. \quad (8)$$

The periodicity of $E_{K,\mathrm{TE}}(x)$ requires that

$$\begin{pmatrix} a_{n-1} \\ b_{n-1} \end{pmatrix}_{\mathrm{TE}}=\exp(iK_{\mathrm{TE}}\Lambda)\begin{pmatrix} a_n \\ b_n \end{pmatrix}_{\mathrm{TE}}, \quad (9)$$

which, by Eq. (7), leads to the eigenequation

$$\begin{bmatrix} A & B \\ C & D \end{bmatrix}_{\mathrm{TE}}\begin{pmatrix} a_n \\ b_n \end{pmatrix}_{\mathrm{TE}}=\exp(iK_{\mathrm{TE}}\Lambda)\begin{pmatrix} a_n \\ b_n \end{pmatrix}_{\mathrm{TE}}. \quad (10)$$

The eigenvalues of Eq. (10) are, using Eqs. (8),

$$\exp(iK_{\mathrm{TE}}\Lambda)=\mathrm{Re}(A_{\mathrm{TE}})\pm\sqrt{[\mathrm{Re}(A_{\mathrm{TE}})]^2-1}, \quad (11)$$

with corresponding eigenvectors

$$\begin{pmatrix} a_n \\ b_n \end{pmatrix}_{\mathrm{TE}}=\begin{bmatrix} B_{\mathrm{TE}} \\ \exp(iK_{\mathrm{TE}}\Lambda)-A_{\mathrm{TE}} \end{bmatrix}=\exp(-in K_{\mathrm{TE}}\Lambda)\begin{pmatrix} a_0 \\ b_0 \end{pmatrix}_{\mathrm{TE}} \quad (12)$$

multiplied by an arbitrary constant (which will hereafter be included in C_2^{TE}). The last term in Eq. (12) follows from repeated application of Eq. (9). As the product of eigenvalues is equal to the determinant (which is unity for a unimodular matrix), the eigenvalues must be the inverse of one another. By summing them, one can find the Bloch wave vector:

$$K_{\mathrm{TE}}=\frac{1}{\Lambda}\cos^{-1}[\mathrm{Re}(A_{\mathrm{TE}})]. \quad (13)$$

Within a unit cell of the cladding, the field components in adjacent slabs are related by the transfer matrix[9]

$$\begin{pmatrix} c_n \\ d_n \end{pmatrix}_{\mathrm{TE}}=\frac{1}{2}\begin{bmatrix} \exp(ik_1a)\left(1+\frac{k_1}{k_2}\right) & \exp(-ik_1a)\left(1-\frac{k_1}{k_2}\right) \\ \exp(ik_1a)\left(1-\frac{k_1}{k_2}\right) & \exp(-ik_1a)\left(1+\frac{k_1}{k_2}\right) \end{bmatrix}\times\begin{pmatrix} a_n \\ b_n \end{pmatrix}_{\mathrm{TE}}. \quad (14)$$

Inserting Eqs. (12) and (6) into Eq. (4) gives the complete form of the field in the waveguide:

$$E_y(x)=\begin{cases} C_1^{\mathrm{TE}}\cos(k_cx), & 0\leqslant x\leqslant\frac{t_c}{2} \\ \quad +b_{0,\mathrm{TE}}\exp\left[-ik_1\left(x-\frac{t_c}{2}-\mathrm{n}\Lambda\right)\right]\Big\}\exp(in K_{\mathrm{TE}}\Lambda), & \\ C_2^{\mathrm{TE}}\Big\{a_{0,\mathrm{TE}}\exp\left[ik_1\left(x-\frac{t_c}{2}-\mathrm{n}\Lambda\right)\right] & \mathrm{n}\Lambda\leqslant\left(x-\frac{t_c}{2}\right)\leqslant\mathrm{n}\Lambda+a \\ \quad +d_{0,\mathrm{TE}}\exp\left[-ik_2\left(x-\frac{t_c}{2}-\mathrm{n}\Lambda-a\right)\right]\Big\}\exp(in K_{\mathrm{TE}}\Lambda), & \\ C_2^{\mathrm{TE}}\Big\{c_{0,\mathrm{TE}}\exp\left[ik_2\left(x-\frac{t_c}{2}-\mathrm{n}\Lambda-a\right)\right] & \mathrm{n}\Lambda+a\leqslant\left(x-\frac{t_c}{2}\right)\leqslant(\mathrm{n}+1)\Lambda \end{cases},$$

$$E_y(-x)=E_y(x). \quad (15)$$

Finally, enforcing continuity of E_y and H_z (proportional to $\partial E_y/\partial x$) at the core–cladding interface leads, via Eqs. (12) and (15), to the mode dispersion equation

$$\frac{1}{k_c}\cot\left(\frac{k_c t_c}{2}\right) = \frac{-i}{k_1}\frac{\exp(iK_{\mathrm{TE}}\Lambda) - A_{\mathrm{TE}} + B_{\mathrm{TE}}}{\exp(iK_{\mathrm{TE}}\Lambda) - A_{\mathrm{TE}} - B_{\mathrm{TE}}}. \quad (16)$$

B. Transverse-Magnetic Polarization

The TM mode contains nonzero field components H_y, E_x, and E_z, where, as before, only one can be considered independent. Here, we solve for H_y and use the curl relation

$$E_x(x) = \frac{\beta}{\omega\epsilon}H_y(x) \quad (17)$$

to determine the electric field normal to the slab interfaces, where ϵ is the dielectric constant, proportional to n^2. The TM mode contains an additional subtlety not encountered in the TE case, in which the ray angle in the cladding may be greater than or less than the external Brewster's angle,

$$\theta_B' = \tan^{-1}\left(\frac{n_2}{n_1}\right). \quad (18)$$

It is important to note that the internal Brewster's angle, $\theta_B = \tan^{-1}(n_1/n_2)$, is not applicable to this discussion, as it exceeds the critical angle for TIR. In terms of transverse propagation vectors, the external Brewster's angle condition corresponds to

$$n_1^2 k_2 = n_2^2 k_1. \quad (19)$$

The phase changes on reflection from each cladding layer shift by a factor of π as the external Brewster's angle is surpassed. As a result, the positions of the nulls and maxima in field amplitude shift by a half-period in the cladding. In particular, the boundary conditions at the core–cladding interface are altered, necessarily changing the symmetry of the fundamental TM mode. When condition (19) holds exactly, the electromagnetic energy is no longer localized, and the TM mode does not exist. This situation is useful in the design of a single-polarization waveguide but will not be explored further.

The field envelope takes the form

$$H_y(x) = \begin{cases} C_1^{\mathrm{TM}}\cos(k_c x), & 0 \le x \le \dfrac{t_c}{2},\ n_1^2 k_2 < n_2^2 k_1 \\ C_1^{\mathrm{TM}}\sin(k_c x), & 0 \le x \le \dfrac{t_c}{2},\ n_1^2 k_2 > n_2^2 k_1 \\ C_2^{\mathrm{TM}} H_{K,\mathrm{TM}}\left(x - \dfrac{t_c}{2}\right)\exp\left[iK_{\mathrm{TM}}\left(x - \dfrac{t_c}{2}\right)\right], & x > \dfrac{t_c}{2} \end{cases},$$

$$H_y(-x) = \begin{cases} H_y(x), & n_1^2 k_2 < n_2^2 k_1 \\ -H_y(x), & n_1^2 k_2 > n_2^2 k_1 \end{cases}, \quad (20)$$

where $H_{K,\mathrm{TM}}(x)$ has the same functional form as $E_{K,\mathrm{TE}}(x)$, but with[9]

$$A_{\mathrm{TM}} = \exp(ik_1 a)\left[\cos k_2 b + \frac{i}{2}\left(\frac{n_2^2 k_1}{n_1^2 k_2} + \frac{n_1^2 k_2}{n_2^2 k_1}\right)\sin k_2 b\right],$$

$$B_{\mathrm{TM}} = \exp(-ik_1 a)\left[\frac{i}{2}\left(\frac{n_2^2 k_1}{n_1^2 k_2} - \frac{n_1^2 k_2}{n_2^2 k_1}\right)\sin k_2 b\right],$$

$$C_{\mathrm{TM}} = B_{\mathrm{TM}}^* D_{\mathrm{TM}} = A_{\mathrm{TM}}^*, \quad (21)$$

$$\begin{pmatrix} c_{\mathrm{n}} \\ d_{\mathrm{n}} \end{pmatrix}_{\mathrm{TM}} = \frac{1}{2}\left(\frac{n_2 k_1}{n_1 k_2}\right) \times \begin{bmatrix} \exp(ik_1 a)\left(1 + \dfrac{n_1^2 k_2}{n_2^2 k_1}\right) & \exp(-ik_1 a)\left(1 - \dfrac{n_1^2 k_2}{n_2^2 k_1}\right) \\ \exp(ik_1 a)\left(1 - \dfrac{n_1^2 k_2}{n_2^2 k_1}\right) & \exp(-ik_1 a)\left(1 + \dfrac{n_1^2 k_2}{n_2^2 k_1}\right) \end{bmatrix} \times \begin{pmatrix} a_{\mathrm{n}} \\ b_{\mathrm{n}} \end{pmatrix}_{\mathrm{TM}}. \quad (22)$$

Continuity of H_y and E_z (proportional to $n^{-2}\partial H_y/\partial x$) at the core–cladding interface leads, via Eqs. (20), to the mode dispersion equation

$$\frac{1}{k_c}\cot\left(\frac{k_c t_c}{2}\right) = \frac{-i}{k_1}\left(\frac{n_1}{n_c}\right)^2 \frac{\exp(iK_{\mathrm{TM}}\Lambda) - A_{\mathrm{TM}} + B_{\mathrm{TM}}}{\exp(iK_{\mathrm{TM}}\Lambda) - A_{\mathrm{TM}} - B_{\mathrm{TM}}}, \quad n_1^2 k_2 < n_2^2 k_1,$$

$$k_c \cot\left(\frac{k_c t_c}{2}\right) = ik_1\left(\frac{n_c}{n_1}\right)^2 \frac{\exp(iK_{\mathrm{TM}}\Lambda) - A_{\mathrm{TM}} - B_{\mathrm{TM}}}{\exp(iK_{\mathrm{TM}}\Lambda) - A_{\mathrm{TM}} + B_{\mathrm{TM}}}, \quad n_1^2 k_2 > n_2^2 k_1. \tag{23}$$

C. Quarter-Wave Condition

We will now enforce the quarter-wave condition within the cladding. This is defined by

$$k_1 a = k_2 b = \pi/2. \tag{24}$$

Inserting Eq. (24) into Eqs. (8) and (21) gives

$$A_{\mathrm{TE}} = D_{\mathrm{TE}} = -\frac{1}{2}\left(\frac{k_2}{k_1} + \frac{k_1}{k_2}\right),$$

$$B_{\mathrm{TE}} = C_{\mathrm{TE}} = \frac{1}{2}\left(\frac{k_2}{k_1} - \frac{k_1}{k_2}\right), \tag{25}$$

$$A_{\mathrm{TM}} = D_{\mathrm{TM}} = -\frac{1}{2}\left(\frac{n_2^2 k_1}{n_1^2 k_2} + \frac{n_1^2 k_2}{n_2^2 k_1}\right),$$

$$B_{\mathrm{TM}} = C_{\mathrm{TM}} = \frac{1}{2}\left(\frac{n_2^2 k_1}{n_1^2 k_2} - \frac{n_1^2 k_2}{n_2^2 k_1}\right) \tag{26}$$

for the QtW-BRW, all real quantities for $n_{\mathrm{eff}} < n_1, n_2$. For both polarizations $|A| > 1$, so by Eq. (13), the Bloch wave vector must have an imaginary component, confirming that the transverse field of the mode does indeed lie in the stop band of the cladding. With Eqs. (25), (26), and (13),

$$K\Lambda = \begin{cases} (2m-1)\pi \pm i \ln\left(\dfrac{k_2}{k_1}\right) & (\mathrm{TE}) \\ (2m-1)\pi \pm i \ln\left(\dfrac{n_2^2 k_1}{n_1^2 k_2}\right) & (\mathrm{TM}) \end{cases}, \tag{27}$$

where $m = 1, 2, \ldots$ is the Bragg order of the cladding. For a first-order cladding, the matrix eigenvalue becomes

$$\exp(iK\Lambda) = \begin{cases} -\left(\dfrac{k_2}{k_1}\right) & (\mathrm{TE}) \\ -\left(\dfrac{n_1^2 k_2}{n_2^2 k_1}\right) & (\mathrm{TM}, n_1^2 k_2 < n_2^2 k_1) \\ -\left(\dfrac{n_2^2 k_1}{n_1^2 k_2}\right) & (\mathrm{TM}, n_1^2 k_2 > n_2^2 k_1) \end{cases}. \tag{28}$$

Note that the sign of $\mathrm{Im}(K\Lambda)$ in Eq. (27) is chosen such that $|\exp(iK\Lambda)| < 1$, necessitated by the physically realizable condition that the field must decay in the cladding. Inserting Eqs. (25), (26), and (28), into Eqs. (16) and (23) shows that the right-hand side of the mode dispersion equation equals zero in the quarter-wave case. Thus, guided modes occur for both polarizations when

$$\frac{k_c t_c}{2} = \frac{(p+1)\pi}{2}, \qquad p = 0, 2, 4, \ldots, \tag{29}$$

where p is the mode order.

We shall concern ourselves with only the fundamental QtW-BRW mode for the remainder of this paper, for which $p = 0$. The derivation of higher-order modes proceeds analogously, although the reader is cautioned that these modes represent a physically different cladding structure, through Eqs. (3) and (24). In this case,

$$k_c = \frac{2\pi}{\lambda}\sqrt{n_c^2 - n_{\mathrm{eff}}^2} = \frac{\pi}{t_c} \tag{30}$$

and thus

$$n_{\mathrm{eff}} = \left[n_c^2 - \left(\frac{\lambda}{2t_c}\right)^2\right]^{1/2}, \tag{31}$$

regardless of polarization, showing that the QtW-BRW is polarization degenerate (for isotropic materials). This result can be justified by examining the QtW-BRW from a ray-optics viewpoint. With TIR guides, form birefringence arises owing to the polarization dependence of the reflection phase at the core–cladding interface. With BRWs, all reflections are either external or internal (with incident angles less than the critical angle for TIR). In both cases, all reflection phases are either zero or π. When the cladding layers have quarter-wave optical thickness, the reflections all sum in phase, the reflection phase from the cladding stack is also either zero or π, and the round-trip sum of reflection phases from both claddings has modulus zero for both polarizations.

It must be noted that the effective index cannot exceed any material indices. If this condition is violated, the field will be evanescent in this material, and quarter-wave thickness can only be asymptotically achieved.[11] In addition, Eq. (31) only results in physically realizable modes when the argument of the square root is positive. These conditions constrain the guide width to

$$\frac{\lambda}{2n_c} < t_c < \frac{\lambda}{2\sqrt{n_c^2 - n_2^2}} \qquad (n_c > n_2),$$

$$\frac{\lambda}{2n_c} < t_c \qquad (n_c < n_2). \tag{32}$$

Once the effective index has been determined, the k_i and cladding layer widths can be calculated using Eqs. (3) and (24), respectively. To fully specify the field envelope, we need only to calculate the field amplitudes in the cladding. Inserting Eqs. (25), (26), and (28) into Eq. (12), we find that the field components in the cladding layer nearest the core (index n_1) satisfy

$$a_0 = -b_0 \qquad (\mathrm{TE,TM}\,[n_1^2k_2 < n_2^2k_1]),$$

$$a_0 = b_0 \qquad (\mathrm{TM}\,[n_1^2k_2 > n_2^2k_1]). \tag{33}$$

In the adjacent cladding layer (index n_2), by Eqs. (14) and (22),

$$c_0 = d_0 = ia_0 \qquad (\mathrm{TE,TM}\,[n_1^2k_2 < n_2^2k_1]),$$

$$c_0 = -d_0 = ia_0 \qquad (\mathrm{TM}\,[n_1^2k_2 > n_2^2k_1]). \tag{34}$$

The absolute magnitude of the field components is not relevant here, as the entire mode will be normalized in Subsection 2.D. Inserting Eqs. (33) and (28) into Eqs. (15) results in

$$E_{\mathrm{TE}}(x) = \begin{cases} C_1^{\mathrm{TE}} \cos(k_c x), & x \leqslant \dfrac{t_c}{2} \\ C_2^{\mathrm{TE}} \left(-\dfrac{k_2}{k_1}\right)^{\mathrm{n}} \sin\left[k_1\left(x - \dfrac{t_c}{2} - \mathrm{n}\Lambda\right)\right], & \mathrm{n}\Lambda \leqslant \left(x - \dfrac{t_c}{2}\right) \leqslant \mathrm{n}\Lambda + a \\ C_2^{\mathrm{TE}} \left(-\dfrac{k_2}{k_1}\right)^{\mathrm{n}} \cos\left[k_2\left(x - \dfrac{t_c}{2} - \mathrm{n}\Lambda - a\right)\right], & \mathrm{n}\Lambda + a \leqslant \left(x - \dfrac{t_c}{2}\right) \leqslant (\mathrm{n}+1)\Lambda \end{cases}, \tag{35}$$

whereas inserting Eqs. (34) and (28) into Eqs. (20) and applying Eq. (17) results in

$$E_{\mathrm{TM}}(x) = \begin{cases} \dfrac{C_1^{\mathrm{TM}}}{n_c^2} \cos(k_c x), & x \leqslant \dfrac{t_c}{2} \\ \dfrac{C_2^{\mathrm{TM}}}{n_1^2} \left(-\dfrac{n_1^2k_2}{n_2^2k_1}\right)^{\mathrm{n}} \sin\left[k_1\left(x - \dfrac{t_c}{2} - \mathrm{n}\Lambda\right)\right], & \mathrm{n}\Lambda \leqslant \left(x - \dfrac{t_c}{2}\right) \leqslant \mathrm{n}\Lambda + a \\ \dfrac{C_2^{\mathrm{TM}}}{n_2^2} \left(-\dfrac{n_1^2k_2}{n_2^2k_1}\right)^{\mathrm{n}} \cos\left[k_2\left(x - \dfrac{t_c}{2} - \mathrm{n}\Lambda - a\right)\right], & \mathrm{n}\Lambda + a \leqslant \left(x - \dfrac{t_c}{2}\right) \leqslant (\mathrm{n}+1)\Lambda \end{cases}, \tag{36}$$

for $n_1^2k_2 < n_2^2k_1$, and

$$E_{\mathrm{TM}}(x) = \begin{cases} \dfrac{C_1^{\mathrm{TM}}}{n_c^2} \sin(k_c x), & x \leqslant \dfrac{t_c}{2} \\ \dfrac{C_2^{\mathrm{TM}}}{n_1^2} \left(-\dfrac{n_2^2k_1}{n_1^2k_2}\right)^{\mathrm{n}} \cos\left[k_1\left(x - \dfrac{t_c}{2} - \mathrm{n}\Lambda\right)\right], & \mathrm{n}\Lambda \leqslant \left(x - \dfrac{t_c}{2}\right) \leqslant \mathrm{n}\Lambda + a \\ -\dfrac{C_2^{\mathrm{TM}}}{n_2^2} \left(-\dfrac{n_2^2k_1}{n_1^2k_2}\right)^{\mathrm{n}} \sin\left[k_2\left(x - \dfrac{t_c}{2} - \mathrm{n}\Lambda - a\right)\right], & \mathrm{n}\Lambda + a \leqslant \left(x - \dfrac{t_c}{2}\right) \leqslant (\mathrm{n}+1)\Lambda \end{cases}, \tag{37}$$

for $n_1^2k_2 > n_2^2k_1$, where the constants β and ω in Eq. (17) have been included in C_1^{TM} and C_2^{TM}. Thus, we see that the Brewster's angle condition (19) separates regimes in which the fundamental TM mode has even or odd symmetry.

D. Normalization

The constants C_1 and C_2 in Eqs. (35)–(37) are determined by the simultaneous conditions that (i) the integrated field intensity $\int |E(x)|^2\,\mathrm{d}x$ must be equal to 1 and (ii) $\partial E(x)/\partial x$ (TE), $n^2 \partial E(x)/\partial x$ (TM, $n_1^2k_2 < n_2^2k_1$), or $n^2E(x)$ (TM, $n_1^2k_2 > n_2^2k_1$) must be continuous at the core–cladding boundary. The usual boundary condition of continuity of $E_{\mathrm{TE}}(x)$ cannot be exploited here, as there is a null at the boundary. Similarly, the usual condition that $n^2 \partial E_{\mathrm{TM}}(x)/\partial x$ is constant at the boundary cannot be applied in the regime $n_1^2k_2 > n_2^2k_1$ as the field has zero derivative, through Eqs. (37) and (29). Condition (ii) requires that

$$C_2 = \begin{cases} -\dfrac{k_c}{k_1} C_1 & (\mathrm{TE,TM}\,[n_1^2k_2 < n_2^2k_1]) \\ C_1, & (\mathrm{TM}\,[n_1^2k_2 > n_2^2k_1]) \end{cases}. \tag{38}$$

To normalize the modes, we set

$$\int_{-\infty}^{\infty} |E(x)|^2 \mathrm{d}x = 2\int_0^{\infty} |E(x)|^2 \mathrm{d}x = 1, \tag{39}$$

where the second integral arises owing to symmetry about the origin. This integral is divided into three parts,

$$I_c + I_1 + I_2 = \frac{1}{2}, \tag{40}$$

where I_c, I_1, and I_2 represent the core, n_1, and n_2 regions, respectively. For TE polarization, in the core,

$$I_c = \int_0^{t_c/2} |C_1^{\mathrm{TE}}|^2 \cos^2(k_c x)\mathrm{d}x = \frac{|C_1^{\mathrm{TE}}|^2 t_c}{4}. \tag{41}$$

In the regions of index n_1,

$$I_1 = |C_2^{\mathrm{TE}}|^2 \sum_{n=0}^{\infty} \int_{t_c/2+n\Lambda}^{t_c/2+n\Lambda+a} \left(-\frac{k_2}{k_1}\right)^{2n} \sin^2\left[k_1\left(x - \frac{t_c}{2} - n\Lambda\right)\right]\mathrm{d}x$$

$$= |C_2^{\mathrm{TE}}|^2 \int_0^a \sin^2(k_1 x)\mathrm{d}x \sum_{n=0}^{\infty} \left(-\frac{k_2}{k_1}\right)^{2n} = \frac{|C_2^{\mathrm{TE}}|^2 a \sigma_{\mathrm{TE}}}{2}, \tag{42}$$

where we have introduced the factor

$$\sigma \equiv \sum_{n=0}^{\infty} \exp(i2K\Lambda) = \begin{cases} \dfrac{k_1^2}{k_1^2 - k_2^2} & (\mathrm{TE}) \\ \dfrac{n_2^4 k_1^2}{n_2^4 k_1^2 - n_1^4 k_2^2} & (\mathrm{TM}, n_1^2 k_2 < n_2^2 k_1) \\ \dfrac{n_1^4 k_2^2}{n_1^4 k_2^2 - n_2^4 k_1^2} & (\mathrm{TM}, n_1^2 k_2 > n_2^2 k_1) \end{cases}, \tag{43}$$

and, likewise,

$$I_2 = \frac{|C_2^{\mathrm{TE}}|^2 b \sigma_{\mathrm{TE}}}{2}. \tag{44}$$

Inserting Eqs. (38) and (41)–(44) into Eq. (40) results in

$$C_1^{\mathrm{TE}} = \left[\frac{t_c}{2} + \frac{\pi k_c^2 \sigma_{\mathrm{TE}}(k_1 + k_2)}{2k_1^3 k_2}\right]^{-1/2}, \tag{45}$$

and, from Eq. (38),

$$C_2^{\mathrm{TE}} = \frac{-k_c}{k_1\left[\dfrac{t_c}{2} + \dfrac{\pi k_c^2 \sigma_{\mathrm{TE}}(k_1 + k_2)}{2k_1^3 k_2}\right]^{1/2}}. \tag{46}$$

For the TM mode, an identical derivation using Eq. (36) gives

$$C_1^{\mathrm{TM}} = \left[\frac{t_c}{2n_c^4} + \frac{\pi k_c^2 \sigma_{\mathrm{TM}}(n_1^4 k_1 + n_2^4 k_2)}{2n_1^4 n_2^4 k_1^3 k_2}\right]^{-1/2}, \tag{47}$$

$$C_2^{\mathrm{TM}} = \frac{-k_c}{k_1\left[\dfrac{t_c}{2n_c^4} + \dfrac{\pi k_c^2 \sigma_{\mathrm{TM}}(n_1^4 k_1 + n_2^4 k_2)}{2n_1^4 n_2^4 k_1^3 k_2}\right]^{1/2}}, \tag{48}$$

for $n_1^2 k_2 < n_2{}^2 k_1$, and

$$C_1^{\mathrm{TM}} = C_2^{\mathrm{TM}} = \left[\frac{t_c}{2n_c^4} + \frac{\pi \sigma_{\mathrm{TM}}(n_1^4 k_1 + n_2^4 k_2)}{2n_1^4 n_2^4 k_1 k_2}\right]^{-1/2}, \tag{49}$$

for $n_1^2 k_2 > n_2{}^2 k_1$.

Field profiles for two QtW-BRWs are shown in Fig. 2, with the waveguide design parameters listed in Table 1. For QtW-BRW #1, $n_1^2 k_2 < n_1^2 k_2$ and, hence, by Eq. (36), the fundamental TM mode is even [Fig. 2(a)]. For QtW-BRW #2 [Fig. 2(b)], $n_1{}^2 k_2 > n_2{}^2 k_1$, and thus the fundamental TM mode is odd, as indicated in Eq. (37). The field profiles are normalized, showing that the TE mode is more local-

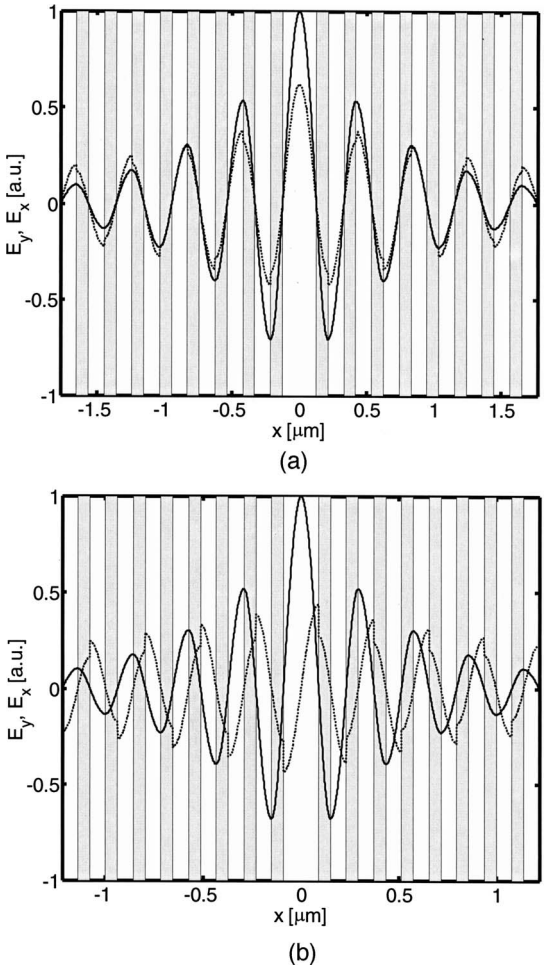

Fig. 2. Field profiles for two different QtW-BRWs. Fields are normalized to show the stronger localization of the TE mode. Waveguide design parameters are listed in Table 1. Solid curve, E_y (TE mode); dotted curve, E_x (TM mode). (a) $n_1^2 k_2 / n_2^2 k_1 = 0.8975$, (b) $n_1^2 k_2 / n_2^2 k_1 = 1.0768$.

Table 1. Waveguide Design Parameters Used in Fig. 2

Parameter	QtW-BRW #1	QtW-BRW #2
n_c	3.25	3.0
n_1	3.6	3.8
n_2	3.3	3.2
t_c (nm)	250	180
λ (μm)	0.775	0.775
a (nm)	88.4	61.1
b (nm)	117.3	79.9
Λ (nm)	205.7	141.0
k_2/k_1	0.7524	0.7636
$n_1^2 k_2 / n_2^2 k_1$	0.8975	1.0768
n_{eff}	2.8566	2.0894

ized near the core. This effect can be explained by noting that the decay factor $|\exp(iK_{TE}\Lambda)| < |\exp(iK_{TM}\Lambda)|$. It has been exploited in the proposal of a polarization splitter based on a directional coupler in non-QtW-BRWs, with a significant polarization dependence of coupling strength.[7] All field profiles have been confirmed by comparison with those found using a fully vectorial, finite-difference mode solver.[12] Having derived a complete set of analytical equations for the field in QtW-BRWs, we shall now study their properties in the remainder of this work.

3. WAVEGUIDE PROPERTIES

A. Overlap Factors

For various applications, such as chemical sensing (within a hollow core), electro-optic or electroabsorptive modulation, or nonlinear frequency conversion, it is desirable to know the fraction of mode power that resides in each material, cladding period, or individual layer. The material power overlap can be determined easily from the overlap integrals. For TE polarization,

$$\Gamma_c^{TE} = (C_1^{TE})^2 t_c/2, \tag{50}$$

$$\Gamma_1^{TE} = (C_1^{TE})^2 \frac{\pi k_c^2 \sigma}{2k_1^3}, \tag{51}$$

$$\Gamma_2^{TE} = (C_1^{TE})^2 \frac{\pi k_c^2 \sigma}{2k_1^2 k_2}, \tag{52}$$

and, for TM polarization,

$$\Gamma_c^{TM} = (C_1^{TM})^2 t_c/2n_c^4, \tag{53}$$

$$\Gamma_1^{TM} = \begin{cases} (C_1^{TM})^2 \dfrac{\pi k_c^2 \sigma}{2n_1^4 k_1^3}, & n_1^2 k_2 < n_2^2 k_1 \\ (C_1^{TM})^2 \dfrac{\pi \sigma}{2n_1^4 k_1}, & n_1^2 k_2 > n_2^2 k_1 \end{cases}, \tag{54}$$

$$\Gamma_2^{TM} = \begin{cases} (C_1^{TM})^2 \dfrac{\pi k_c^2 \sigma}{2n_2^4 k_1^2 k_2}, & n_1^2 k_2 < n_2^2 k_1 \\ (C_1^{TM})^2 \dfrac{\pi \sigma}{2n_2^4 k_2}, & n_1^2 k_2 > n_2^2 k_1 \end{cases}. \tag{55}$$

The reader may easily verify that, for both polarizations, $\Gamma_c + \Gamma_1 + \Gamma_2 = 1$, as required.

The power fraction in the layer with index $n_i (i = 1, 2)$ in the nth unit cell of the cladding (considering the upper and lower claddings separately) is equal to

$$\Gamma_i^{TE,n} = \frac{\Gamma_i^{TE}}{2\sigma}\left(\frac{k_2}{k_1}\right)^{2n} = \frac{\Gamma_i^{TE}}{2}\left[\left(\frac{k_2}{k_1}\right)^{2n} - \left(\frac{k_2}{k_1}\right)^{2n+2}\right], \tag{56}$$

$$\Gamma_i^{TM,n} = \begin{cases} \dfrac{\Gamma_i^{TM}}{2\sigma}\left(\dfrac{n_1^2 k_2}{n_2^2 k_1}\right)^{2n} = \dfrac{\Gamma_i^{TM}}{2}\left[\left(\dfrac{n_1^2 k_2}{n_2^2 k_1}\right)^{2n} - \left(\dfrac{n_1^2 k_2}{n_2^2 k_1}\right)^{2n+2}\right] & (n_1^2 k_2 < n_2^2 k_1) \\ \dfrac{\Gamma_i^{TM}}{2\sigma}\left(\dfrac{n_2^2 k_1}{n_1^2 k_2}\right)^{2n} = \dfrac{\Gamma_i^{TM}}{2}\left[\left(\dfrac{n_2^2 k_1}{n_1^2 k_2}\right)^{2n} - \left(\dfrac{n_2^2 k_1}{n_1^2 k_2}\right)^{2n+2}\right] & (n_1^2 k_2 > n_2^2 k_1) \end{cases}. \tag{57}$$

To estimate power leakage through a finite cladding, it is useful to calculate the power in the first N unit cells of one cladding. Assuming that N is large enough such that the finite cladding does not appreciably alter the mode profile, we use the partial sum

$$\Gamma^{TE,N} = \frac{(\Gamma_1^{TE} + \Gamma_2^{TE})}{2\sigma}\sum_{n=0}^{N-1}\left(\frac{k_2}{k_1}\right)^{2n} = \frac{(\Gamma_1^{TE} + \Gamma_2^{TE})}{2}\left[1 - \left(\frac{k_2}{k_1}\right)^{2N}\right], \tag{58}$$

$$\Gamma^{TM,N} = \begin{cases} \dfrac{(\Gamma_1^{TM} + \Gamma_2^{TM})}{2}\left[1 - \left(\dfrac{n_1^2 k_2}{n_2^2 k_1}\right)^{2N}\right] & (n_1^2 k_2 < n_2^2 k_1) \\ \dfrac{(\Gamma_1^{TM} + \Gamma_2^{TM})}{2}\left[1 - \left(\dfrac{n_2^2 k_1}{n_1^2 k_2}\right)^{2N}\right] & (n_1^2 k_2 > n_2^2 k_1) \end{cases}. \tag{59}$$

The simplicity of calculating the overlap integrals in any given layer within the structure as shown above demon-

strates the power of the analytical approach taken here. This lends itself as a powerful design tool for optimizing structures or devices or both based on QtW-BRWs with relative ease and speed. In contrast, with most other waveguide structures, the field has to be calculated for every set of parameters, and an overlap integral needs to be evaluated to obtain similar figures.

B. Propagation Loss

The preceding derivation of the mode dispersion equation operated on the assumption that the cladding consists of an infinite number of periods. For a mode that lies within the cladding stop band, this results in no leakage during propagation. For practical devices, however, there will be a finite number of cladding periods. In this subsection, we describe a method of estimating the resulting loss. We assume that the loss is low enough that the propagation constant β is essentially real and that there is negligible perturbation to the unit-cell translation matrix formulation described in Section 2.

The leakage in such devices can be estimated using a ray-optics approach.[13] In the ray-optics picture, the angle of incidence between core and cladding is given by

$$\theta_i = \sin^{-1}\left(\frac{n_{\text{eff}}}{n_c}\right) = \sin^{-1}\left\{\left[1 - \left(\frac{\lambda}{2n_c t_c}\right)^2\right]^{1/2}\right\}, \quad (60)$$

and the number of reflections per unit length is $1/(t_c \tan\theta_i)$. The reflection coefficient at the interface between the core and the finite cladding can be calculated using the transfer-matrix method of Chilwell and Hodgkinson.[14]

In the transfer-matrix method, a unimodular field-transfer matrix $\mathbf{M}_j$ relates the field components in two mutually orthogonal directions (both parallel to the slab interfaces), between two adjacent layers,

$$\mathbf{M}_j = \begin{bmatrix} \cos k_j t_j & -(i/\gamma_j)\sin k_j t_j \\ -i\gamma_j \sin k_j t_j & \cos k_j t_j \end{bmatrix}, \quad (61)$$

where

$$\gamma_j = \frac{1}{(n_j)^{2\rho}}\sqrt{n_j^2 - n_{\text{eff}}^2}, \qquad \rho = \begin{cases} 0 & \text{(TE)} \\ 1 & \text{(TM)} \end{cases} \quad (62)$$

and t_j is the physical thickness of the layer. The transfer matrix for a multilayer stack is given by the product of these matrices,

$$\mathbf{M} = \prod_j \mathbf{M}_j = \begin{bmatrix} m_{11} & m_{12} \\ m_{21} & m_{22} \end{bmatrix}, \quad (63)$$

from which the reflection coefficient can be calculated as

$$r = \frac{\gamma_c m_{11} + \gamma_c\gamma_s m_{12} - m_{21} - \gamma_s m_{22}}{\gamma_c m_{11} + \gamma_c\gamma_s m_{12} + m_{21} + \gamma_s m_{22}}, \quad (64)$$

where γ_c and γ_s are defined analogously to Eq. (62) for the core and substrate, respectively.

For the QtW-BRW, the cladding at $x>0$ can be expressed as

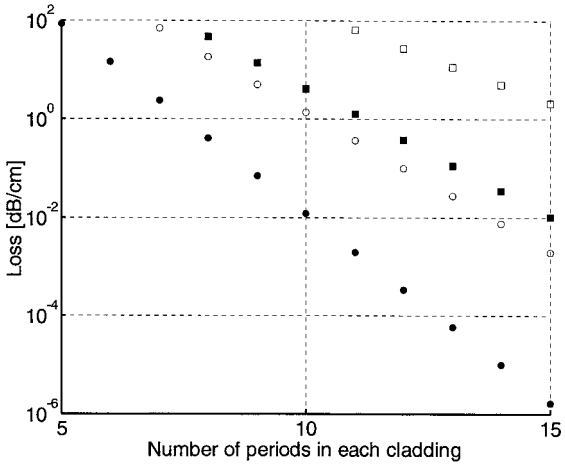

Fig. 3. Propagation loss in a QtW-BRW. Filled symbols, $n_1-n_2=0.5$; open symbols, $n_1-n_2=0.4$. Circles, TE; squares, TM.

$$\mathbf{M} = (\mathbf{M}_1\mathbf{M}_2)^N = \left(\begin{bmatrix} 0 & -i/\gamma_1 \\ -i\gamma_1 & 0 \end{bmatrix}\begin{bmatrix} 0 & -i/\gamma_2 \\ -i\gamma_2 & 0 \end{bmatrix}\right)^N = (-1)^N\begin{bmatrix} (\gamma_2/\gamma_1)^N & 0 \\ 0 & (\gamma_1/\gamma_2)^N \end{bmatrix}, \quad (65)$$

leading to a reflection coefficient of

$$r = \frac{\gamma_c\left(\frac{\gamma_2}{\gamma_1}\right)^N - \gamma_s\left(\frac{\gamma_1}{\gamma_2}\right)^N}{\gamma_c\left(\frac{\gamma_2}{\gamma_1}\right)^N + \gamma_s\left(\frac{\gamma_1}{\gamma_2}\right)^N}. \quad (66)$$

The power remaining after each reflection is $|r|^2$. We can now calculate the propagation loss by using Eqs. (60)–(66):

$$\text{Loss (decibels per centimeter)} = \frac{-\lambda \ln|r|}{10n_c t_c^2\left[1 - \left(\frac{\lambda}{2n_c t_c}\right)^2\right]^{1/2}}. \quad (67)$$

Plots of propagation loss versus N for $\{n_c, n_1, n_2, n_s\} = \{3.5, 3.75, 3.25, 3.75\}$, $t_c = 250$ nm, and $\lambda = 775$ nm are shown in Fig. 3. As expected, loss decreases exponentially with N, approaching negligible values after just a few periods, and leakage of the TM mode is much greater than that of the TE mode. A second QtW-BRW with $\{n_c, n_1, n_2, n_s\} = \{3.5, 3.7, 3.3, 3.7\}$ is shown on the same plot. The smaller index difference in the cladding results in a substantial increase in propagation loss. These results indicate that practical structures can be considered essentially lossless, contrary to the conclusions of previous authors.[15]

C. Dispersion

The dispersion of effective index with wavelength is a significant factor in the design of many resonant[6] or nonlinear[5] devices. Chromatic dispersion of the nominally

Q+W-BRW is analyzed by the first-order perturbation theory derived in Appendix A. Let the perturbed indices be denoted

$$\tilde{n}_i = n_i + \Delta n_i. \tag{68}$$

Then the perturbed transverse propagation vectors are equal to

$$\begin{aligned}\tilde{k}_i &= k_i + \Delta k_i \\ &= \left(\frac{2\pi}{\lambda + \Delta\lambda}\right)\sqrt{(n_i + \Delta n_i)^2 - (n_{\text{eff}} + \Delta n_{\text{eff}})^2} \\ &\approx \frac{2\pi}{\lambda}\left(1 - \frac{\Delta\lambda}{\lambda}\right)\sqrt{n_i^2 - n_{\text{eff}}^2}\left(1 + \frac{n_i\Delta n_i - n_{\text{eff}}\Delta n_{\text{eff}}}{n_i^2 - n_{\text{eff}}^2}\right),\end{aligned} \tag{69}$$

where λ is the nominal (quarter-wave) wavelength, from which we see that, to first order,

$$\begin{aligned}\Delta k_i &\approx k_i\left(\frac{n_i\Delta n_i - n_{\text{eff}}\Delta n_{\text{eff}}}{n_i^2 - n_{\text{eff}}^2} - \frac{\Delta\lambda}{\lambda}\right) \\ &= F_i\Delta\lambda - k_i\left(\frac{n_{\text{eff}}\Delta n_{\text{eff}}}{n_i^2 - n_{\text{eff}}^2} + \frac{\Delta\lambda}{\lambda}\right),\end{aligned} \tag{70}$$

where

$$F_i \equiv \frac{k_0^2 n_i \dfrac{\partial n_i}{\partial\lambda}}{k_i} \tag{71}$$

is a term proportional to the chromatic dispersion of a particular waveguide material. Inserting expression (70) into Eq. (A10) and rearranging terms give the chromatic dispersion

$$\frac{\Delta n_{\text{eff}}}{\Delta\lambda} = \frac{\dfrac{\pi k_c}{t_c(k_2^2 - k_1^2)}[F_1 + F_2 - (k_1 + k_2)\lambda^{-1}] - F_c + k_c\lambda^{-1}}{k_0^2 n_{\text{eff}}\left[\dfrac{\pi k_c}{t_c k_1 k_2(k_2 - k_1)} - \dfrac{1}{k_c}\right]}. \tag{72}$$

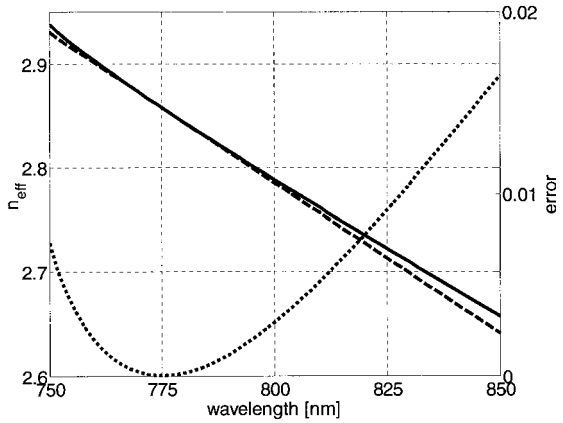

Fig. 4. Chromatic dispersion of the BRW mode, effective index versus wavelength (nominally quarter wave at $\lambda = 775$ nm). Solid curve, numerical dispersion curve; dashed curve, analytical (linear) model from Eq. (72); dotted curve, error in analytical model.

To investigate the range of applicability of this linear approximation, we model a waveguide in $Al_xGa_{1-x}As$. The waveguide is a quarter wave at a wavelength of 775 nm. The aluminum fraction in the core is $x_c = 65\%$, whereas in the cladding, $x_1 = 20\%$ and $x_2 = 58\%$. The core thickness is 250 nm. This waveguide approximates QtW-BRW #1 but includes material dispersion of AlGaAs, which is modeled after Adachi.[16] By Eq. (72), the dispersion is calculated as $\Delta n_{\text{eff}}/\Delta\lambda = -2.89 \times 10^{-3}$ nm^{-1}. Figure 4 compares the effective index modeled using the mode dispersion equation (16) with the linear approximation. As expected, the residual error is parabolic in the vicinity of 775 nm and is less than 0.01 across a range of over 80 nm. One can further reduce this error by employing a second-order approximation to the material dispersion, particularly in the spectral region under consideration here, which is near the bandgap of the AlGaAs alloys used. The procedure detailed here suggests how the waveguide dispersion can be tuned by one's adjusting the relative composition of the core and cladding layers of the QtW-BRW. This tuning can take place without affecting the propagation losses or the field profile and may have many applications in nonlinear optics. For instance, soliton propagation relies on the balance between third-order nonlinearities and the waveguide dispersion. Controlling dispersion could be used to lower the zero-order soliton threshold. This will lead to achieving solitonlike effects such as switching, limiting, and particlelike temporal pulse robustness at lower intensities.

4. TUNING

Waveguide device functionality is expanded by the ability to tune the effective index of the guided mode. The tuning mechanism can take many forms, depending on the type of material: altering the core thickness in an air-core BRW,[6] changing the index of one or more layers by carrier injection or electro-optic means in a semiconductor BRW,[5] or thermo-optic tuning, just to name a few. In all cases, we can consider tuning away from the quarter-wave condition by the perturbation method described in Appendix A.

Here we consider a waveguide in which only the core index is altered, as might be encountered in a p-i-n structure in $Al_xGa_{1-x}As$. In this case, the propagation vectors in the cladding become

$$\tilde{k}_i = k_i + \Delta k_i = \left(\frac{2\pi}{\lambda}\right)\sqrt{n_i^2 - (n_{\text{eff}} + \Delta n_{\text{eff}})^2} \approx k_i\left(1 - \frac{n_{\text{eff}}\Delta n_{\text{eff}}}{n_i^2 - n_{\text{eff}}^2}\right) \tag{73}$$

($i = 1, 2$), which results in

$$\Delta k_i = \frac{-k_0^2 n_{\text{eff}}\Delta n_{\text{eff}}}{k_i}. \tag{74}$$

In the core,

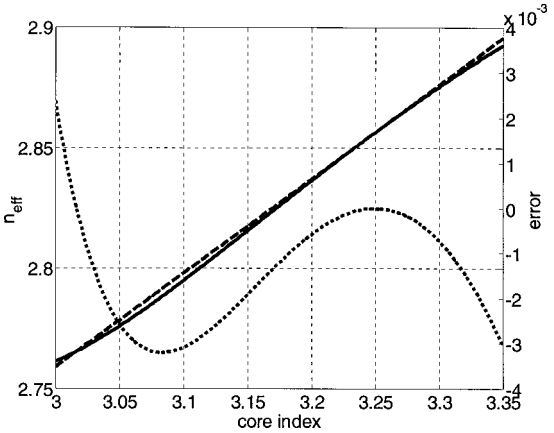

Fig. 5. Effective index versus core index for a BRW waveguide (nominally quarter wave at $n_c=3.25$). Solid curve, numerical tuning curve; dashed curve, analytical (linear) model from Eq. (76); dotted curve, error in analytical model.

$$\tilde{k}_c = \left(\frac{2\pi}{\lambda}\right)\sqrt{(n_c+\Delta n_c)^2-(n_{\text{eff}}+\Delta n_{\text{eff}})^2},$$

$$\Delta k_c \approx \left(\frac{k_0^2}{k_c}\right)(n_c\Delta n_c - n_{\text{eff}}\Delta n_{\text{eff}}). \tag{75}$$

Inserting expressions (74) and (75) into Eq. (A10) and rearranging terms give

$$\frac{\Delta n_{\text{eff}}}{\Delta n_c} = \frac{n_c}{n_{\text{eff}}}\left[1+\frac{\pi k_c^2(k_2+k_1)}{t_c k_1 k_2(k_1^2-k_2^2)}\right]^{-1}. \tag{76}$$

As an example, we use a nominal structure identical to QtW-BRW #1 (see Table 1). The core index is tuned from 3.0 to 3.35. A linear tuning rate of $\Delta n_{\text{eff}}/\Delta n_c=0.391$ was calculated using Eq. (76), and, as Fig. 5 indicates, the linear approximation is accurate to within $\sim 3\times 10^{-4}$ over this range. The tuning capability demonstrated here provides some insight into the practicality of these waveguides. Although they rely on resonance effects, due to finite fabrication tolerances, these resonances can deviate from the design values. The demonstrated tuning ability can be used to ensure that the desired operating conditions are accessible.

Note that the method described above gives a result identical to that found using Schrödinger perturbation theory.[17] In this theory, a small change in core index causes a corresponding first-order change in propagation constant:

$$\Delta(\beta^2) \approx \frac{k_0^2\int_{\text{core}}\Delta n^2(x)|E(x)|^2dx}{\int_{-\infty}^{\infty}|E(x)|^2dx} = k_0^2\Delta n_c^2\Gamma_c, \tag{77}$$

which, by using Eq. (50), is equivalent to Eq. (76). This justifies the application of our method in calculating the dispersion as in Subsection 3.C.

5. QUARTER-WAVE BRAGG REFLECTION WAVEGUIDE–TOTAL-INTERNAL-REFLECTION CHANNEL WAVEGUIDE

For most practical devices, a waveguide must provide confinement in the transverse (y) direction as well. This is easily accomplished in cylindrical Bragg fibers using a radial grating[18] but is difficult to achieve using planar fabrication processes. In this section, we investigate the effect of using TIR for transverse confinement, as depicted in Fig. 6. The waveguide under consideration is QtW-BRW #1 with 20 cladding periods on either side of the core, and we investigate waveguide widths between 0.8 and 5.0 μm. We assume that the waveguide is surrounded by air and calculate the modes by using a semivectorial finite-difference method.[19] Figure 7 shows the effective indices of the first three modes as a function of width. The modal subscripts (q,p) denote the transverse (TIR) mode number and lateral (BRW) mode number, respectively. Here, $p=0$ to indicate the fundamental BRW mode. For increasing width, the effective indices approach that of the slab guide, indicated by a horizontal line on the plot. The confinement-induced birefringence favors the TM mode and decreases with width. Figure 8 shows the intensity of the first two modes at each polarization for the 3 μm waveguide. Confinement in the core is much stronger in the TE case, as explained in Subsection 3.B.

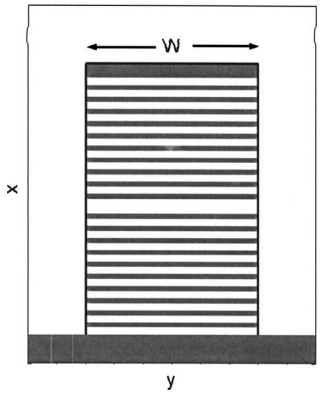

Fig. 6. Channel waveguide, utilizing Bragg waveguiding in the lateral direction and total internal reflection in the transverse direction.

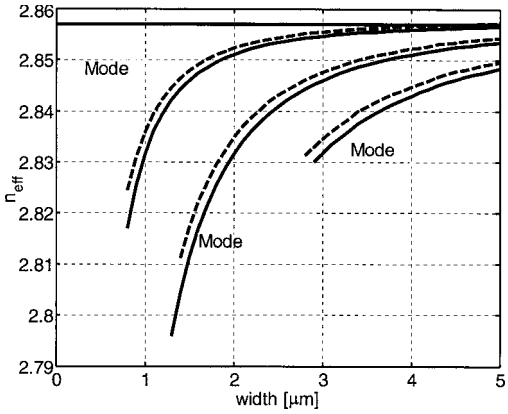

Fig. 7. Effective index versus waveguide width: QtW-BRW #1. Solid curve, TE; dashed curve, TM. The horizontal line at $n_{\text{eff}}=2.8566$ represents the slab waveguide.

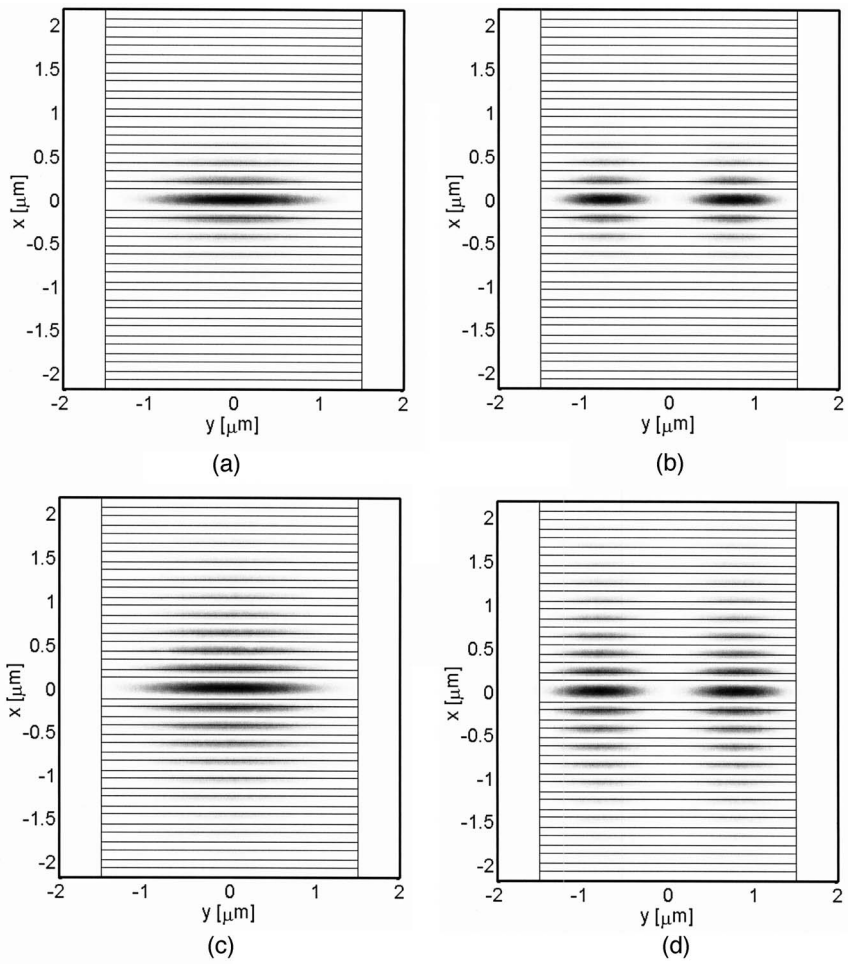

Fig. 8. Mode intensity, QtW-BRW #1, 3 μm width. (a) TE_{00}, (b) TE_{10}, (c) TM_{00}, (d) TM_{10}. The waveguide geometry is superimposed on the figure.

6. DISCUSSION AND SUMMARY

We have derived analytical expressions for the electric field in a one-dimensional quarter-wave Bragg reflection waveguide. These formulas have been confirmed by comparison with numerical simulations and provide additional physical insight into the waveguiding properties. It was shown that such structures are polarization degenerate with greater core confinement of the TE mode. This lack of birefringence suggests that the QtW-BRW shows great promise for utilization in polarization-independent devices. In particular, the efficiency of parametric down-conversion for generation of entangled photons in a type-II (orthogonal polarization) process stands to increase. The analysis has also identified two distinct regimes of TM operation, characterized by a reversal in the mode symmetry. This phenomenon suggests the possibility of achieving robustly single-polarization devices.

With a first-order expansion, dispersion and tuning curves about the quarter-wave point have been derived. The effect of transverse confinement by total internal reflection has also been investigated, indicating a lifting of the degeneracy to favor the TM mode. This introduces the prospect of a waveguide that supports only the TM polarization, a phenomenon that is difficult to achieve using TIR waveguides. Although the transverse confinement in this study was provided by TIR at an interface with air, it is, of course, possible to provide transverse confinement through a two-dimensional photonic bandgap cladding. Much work has been done on defect-line waveguides in a two-dimensional photonic bandgap structure in which lateral confinement is provided by TIR.[20] It is anticipated that utilizing Bragg waveguiding in the lateral direction will introduce additional freedom in tailoring the dispersive properties of the waveguide.

APPENDIX A: PERTURBATION OF THE MODE CONDITION EQUATION

To estimate such waveguide properties as dispersion and tuning curves, it is necessary to explore the deviation of the mode dispersion equation from the ideal quarter-wave case. This is accomplished by adding a perturbation term Δk_i to each propagation vector, with subsequent expansion of the resulting equation to first order in the perturbations. The result will be a mode detuning equation, linear in Δk_i, that is independent of the source of the perturbation and whose solution can be rearranged to determine the waveguide property under consideration. Here, we outline this procedure for the TE mode only; the TM mode follows a similar analysis. Note that, as the po-

larization degeneracy is lifted when the waveguide is tuned away from the quarter-wave condition, the k_i become polarization dependent by Eq. (3). We will omit the subscripts for brevity. Polarization subscripts for matrix elements will remain, however, to indicate that their defining equations are unique to a specific polarization.

The perturbed mode dispersion equation (16) is written as

$$\frac{1}{k_c+\Delta k_c}\cot\left[\frac{(k_c+\Delta k_c)t_c}{2}\right]=\frac{-i}{k_1+\Delta k_1}\left(\frac{\{\exp(iK_{\mathrm{TE}}\Lambda)+\Delta[\exp(iK_{\mathrm{TE}}\Lambda)]\}-(A_{\mathrm{TE}}+\Delta A_{\mathrm{TE}})+(B_{\mathrm{TE}}+\Delta B_{\mathrm{TE}})}{\{\exp(iK_{\mathrm{TE}}\Lambda)+\Delta[\exp(iK_{\mathrm{TE}}\Lambda)]\}-(A_{\mathrm{TE}}+\Delta A_{\mathrm{TE}})-(B_{\mathrm{TE}}+\Delta B_{\mathrm{TE}})}\right). \tag{A1}$$

Expanding the left-hand side of Eq. (A1) to first order about the nominal quarter-wave condition results in

$$\frac{1}{k_c+\Delta k_c}\cot\left[\frac{(k_c+\Delta k_c)t_c}{2}\right]\approx\frac{1}{k_c}\left(1-\frac{\Delta k_c}{k_c}\right)\left(\frac{-\Delta k_c t_c}{2}\right)\approx\frac{-\Delta k_c t_c}{2k_c}, \tag{A2}$$

and the right-hand side is expanded as

$$\begin{aligned}&\frac{-i}{k_1}\left(1-\frac{\Delta k_1}{k_1}\right)\left[\frac{\exp(iK_{\mathrm{TE}}\Lambda)-A_{\mathrm{TE}}+B_{\mathrm{TE}}}{\exp(iK_{\mathrm{TE}}\Lambda)-A_{\mathrm{TE}}-B_{\mathrm{TE}}}\right]\\&\quad\times\left\{1+\frac{\Delta[\exp(iK_{\mathrm{TE}}\Lambda)]-\Delta A_{\mathrm{TE}}+\Delta B_{\mathrm{TE}}}{\exp(iK_{\mathrm{TE}}\Lambda)-A_{\mathrm{TE}}+B_{\mathrm{TE}}}-\frac{\Delta[\exp(iK_{\mathrm{TE}}\Lambda)]-\Delta A_{\mathrm{TE}}-\Delta B_{\mathrm{TE}}}{\exp(iK_{\mathrm{TE}}\Lambda)-A_{\mathrm{TE}}-B_{\mathrm{TE}}}\right\}\\&\quad\approx\frac{-i}{k_1}\left\{\frac{\Delta[\exp(iK_{\mathrm{TE}}\Lambda)]-\Delta A_{\mathrm{TE}}+\Delta B_{\mathrm{TE}}}{\exp(iK_{\mathrm{TE}}\Lambda)-A_{\mathrm{TE}}-B_{\mathrm{TE}}}\right\},\end{aligned} \tag{A3}$$

where we have made use of the fact that $\exp(iK_{\mathrm{TE}}\Lambda)-A_{\mathrm{TE}}+B_{\mathrm{TE}}=0$. Next, we use the perturbed k_i to calculate the transfer-matrix elements by using Eqs. (8),

$$\begin{aligned}\tilde{A}_{\mathrm{TE}}&=A_{\mathrm{TE}}+\Delta A_{\mathrm{TE}}\\&=\exp[i(k_1+\Delta k_1)a]\left\{\cos[(k_2+\Delta k_2)b]+\frac{i}{2}\left(\frac{k_2+\Delta k_2}{k_1+\Delta k_1}+\frac{k_1+\Delta k_1}{k_2+\Delta k_2}\right)\sin[(k_2+\Delta k_2)b]\right\}\\&\approx i(1+i\Delta k_1 a)\left[-\Delta k_2 b+\frac{i}{2}\left(\frac{k_2}{k_1}+\frac{k_1}{k_2}\right)\times\left(1+\frac{2k_2\Delta k_2+2k_1\Delta k_1}{k_2^2+k_1^2}-\frac{\Delta k_1}{k_1}-\frac{\Delta k_2}{k_2}\right)\right],\end{aligned} \tag{A4}$$

which, when compared with Eqs. (25), results in

$$\Delta A_{\mathrm{TE}}=\Delta k_1\left[\frac{1}{2k_1}\left(\frac{k_2}{k_1}+\frac{k_1}{k_2}\right)-\frac{1}{k_2}-i\left(\frac{\pi}{4k_1}\right)\left(\frac{k_2}{k_1}+\frac{k_1}{k_2}\right)\right]+\Delta k_2\left[\frac{1}{2k_2}\left(\frac{k_2}{k_1}+\frac{k_1}{k_2}\right)-\frac{1}{k_1}-i\left(\frac{\pi}{2k_2}\right)\right]. \tag{A5}$$

In Eq. (A5), the relation (24) has been used. A similar analysis gives

$$\Delta B_{\mathrm{TE}}=\Delta k_1\left[\frac{-1}{2k_1}\left(\frac{k_2}{k_1}-\frac{k_1}{k_2}\right)-\frac{1}{k_2}-i\left(\frac{\pi}{4k_1}\right)\left(\frac{k_2}{k_1}-\frac{k_1}{k_2}\right)\right]+\Delta k_2\left[\frac{-1}{2k_2}\left(\frac{k_2}{k_1}-\frac{k_1}{k_2}\right)+\frac{1}{k_1}\right], \tag{A6}$$

and it is easily shown that

$$\Delta D_{\mathrm{TE}}=\Delta A_{\mathrm{TE}}^{*},\qquad \Delta C_{\mathrm{TE}}=\Delta B_{\mathrm{TE}}^{*}. \tag{A7}$$

This allows us to introduce a perturbation matrix

$$\Xi_{\mathrm{TE}}=\begin{bmatrix}\Delta A_{\mathrm{TE}} & \Delta B_{\mathrm{TE}}\\ \Delta B_{\mathrm{TE}}^{*} & \Delta A_{\mathrm{TE}}^{*}\end{bmatrix}. \tag{A8}$$

The matrix eigenvalue now contains a perturbation term that is easily calculated as[21]

$$\begin{aligned}\Delta[\exp(iK_{\mathrm{TE}}\Lambda)]&=\langle u_{\mathrm{TE}}^{+},\Xi_{\mathrm{TE}}u_{\mathrm{TE}}^{+}\rangle\\&=\frac{1}{2}[-1\quad 1]\begin{bmatrix}\Delta A_{\mathrm{TE}} & \Delta B_{\mathrm{TE}}\\ \Delta B_{\mathrm{TE}}^{*} & \Delta A_{\mathrm{TE}}^{*}\end{bmatrix}\begin{pmatrix}-1\\1\end{pmatrix}\\&=\mathrm{Re}(\Delta A_{\mathrm{TE}}-\Delta B_{\mathrm{TE}}),\end{aligned} \tag{A9}$$

where u_{TE}^{+} is the normalized eigenvector of the unperturbed transfer matrix corresponding to eigenvalue $\exp(iK_{\mathrm{TE}}\Lambda)$, given by Eqs. (33). With Eqs. (25), (28), (A5), (A6), and (A9), expressions (A2) and (A3) reduce to the mode detuning equation

$$\Delta k_c=\frac{\pi k_c(\Delta k_1+\Delta k_2)}{t_c(k_2^2-k_1^2)}. \tag{A10}$$

ACKNOWLEDGMENTS

This work has been supported by the Department of Electrical and Computer Engineering at the University of Toronto and the Natural Sciences and Engineering Research Council, Canada.

Brian R. West, the corresponding author, can be reached at the address on the title page or by phone, 1-416-946-8663, or e-mail, brian.west@utoronto.ca.

REFERENCES

1. P. Yeh and A. Yariv, "Bragg reflection waveguides," Opt. Commun. **19**, 427–430 (1976).
2. P. Yeh, A. Yariv, and C.-S. Hong, "Electromagnetic propagation in periodic stratified media. I. General theory," J. Opt. Soc. Am. **67**, 428–438 (1977).

3. A. Mizrahi and L. Schachter, "Optical Bragg accelerators," Phys. Rev. E **70**, 016505 (2004).
4. Z. Zhang, S. G. Tantawi, and R. D. Ruth, "Distributed grating-assisted coupler for optical all-dielectric electron accelerator," Phys. Rev. ST Accel. Beams **8**, 071302 (2005).
5. A. S. Helmy and B. R. West, "Phase matching using Bragg reflector waveguides," in *Proceedings of the 18th Annual Meeting of the IEEE Lasers and Electro-Optics Society* (IEEE, 2005), pp. 424–425.
6. Y. Sakurai and F. Koyama, "Proposal of tunable hollow waveguide distributed Bragg reflectors," Jpn. J. Appl. Phys. Part 1 **43**, L631–L633 (2004).
7. E. Simova and I. Golub, "Polarization splitter/combiner in high index contrast Bragg reflector waveguides," Opt. Express **11**, 3425–3430 (2003).
8. C. Wächter, F. Lederer, L. Leine, U. Trutschel, and M. Mann, "Nonlinear Bragg reflection waveguide," J. Appl. Phys. **71**, 3688–3692 (1992).
9. P. Yeh, *Optical Waves in Layered Media* (Wiley, 2005).
10. P. Kwiat, K. Mattle, H. Weinfurter, A. Zeilinger, A. Sergienko, and Y. Shih, "New high-intensity source of polarization-entangled photon pairs," Phys. Rev. Lett. **75**, 4337–4341 (1995).
11. S. Esposito, "Universal photonic tunneling time," Phys. Rev. E **64**, 026609 (2001).
12. Mode Solutions version 1.0, Lumerical Solutions, Inc., www.lumerical.com.
13. A. Argyros, "Guided modes and loss in Bragg fibres," Opt. Express **10**, 1411–1417 (2002).
14. J. Chilwell and I. Hodgkinson, "Thin-films field-transfer matrix theory of planar multilayer waveguides and reflection from prism-loaded waveguides," J. Opt. Soc. Am. A **1**, 742–753 (1984).
15. P. M. Lambkin and K. A. Shore, "Nonlinear semiconductor Bragg reflection waveguide structures," IEEE J. Quantum Electron. **27**, 824–829 (1991).
16. S. Adachi, "GaAs, AlAs, and $Al_xGa_{1-x}As$ material parameters for use in research and device applications," J. Appl. Phys. **58**, R1–R29 (1985).
17. J. J. Sakurai, *Modern Quantum Mechanics*, rev. ed. (Addison-Wesley, 1994).
18. P. Yeh, A. Yariv, and E. Marom, "Theory of Bragg fiber," J. Opt. Soc. Am. **68**, 1196–1201 (1978).
19. C. M. Kim and R. V. Ramaswamy, "Modeling of graded-index channel waveguides using nonuniform finite-difference method," J. Lightwave Technol. **7**, 1581–1589 (1989).
20. Y. Sugimoto, Y. Tanaka, N. Ikeda, Y. Nakamura, K. Asakawa, and K. Inoue, "Low propagation loss of 0.76 dB/mm in GaAs-based single-line-defect two-dimensional photonic crystal slab waveguides up to 1 cm in length," Opt. Express **12**, 1090–1096 (2004).
21. A. S. Deif, *Advanced Matrix Theory for Scientists and Engineers* (Routledge, 1987).